Titre: Title:	Natural convection in a rectangular cavity with wall temperature decreasing at a uniform rate
Auteurs: Authors:	Patrick Vasseur, & Luc Robillard
Date:	1981
Type:	Rapport / Report
Référence: Citation:	Vasseur, P., & Robillard, L. (1981). Natural convection in a rectangular cavity with wall temperature decreasing at a uniform rate. (Rapport technique n° EP-R-81-01). https://publications.polymtl.ca/6181/

Institution:	École Polytechnique de Montréal
Numéro de rapport: Report number:	EP-R-81-01
URL officiel: Official URL:	
Mention légale: Legal notice:	

SERVICES DE LA RECHERCHE

Rapport technique EP 81-R-1
Classification: Library of Congress No ...

NATURAL CONVECTION IN A RECTANGULAR CAVITY WITH WALL TEMPERATURE DECREASING AT A UNIFORM RATE

by

P. Vasseur and L. Robillard

January 1981

Ecole Polytechnique de Montréal

Campus de l'Université
de Montréal
Case postale 6079
Succursale 'A'
Montréal, Québec
H3C 3A7

NATURAL CONVECTION IN A RECTANGULAR CAVITY WITH WALL TEMPERATURE DECREASING AT A UNIFORM RATE

by

P. VASSEUR AND L. ROBILLARD

Ecole Polytechnique, Université de Montréal
Department of Civil Engineering
Montréal, Québec, Canada H3C 3A7

ABSTRACT

The transient natural convection in a fluid contained in a rectangular enclosure, the wall of which is maintained at a uniform temperature which changes at a steady rate, is approached by a numerical method. The time-dependent governing differential equations are solved using an alternating implicit finite difference method. Numerical solutions are obtained for $Pr = 0.73$, 7.3 and 73 and a range of Rayleigh numbers $R_a = 10^2 \sim 10^8$. The transient flow and temperature fields, local and overall heat rate are presented. Although the present problem is transient, a quasi-steady state develops if the cooling rate applied to the wall of the cavity is held constant long enough. For quasi-steady state, a generalized correlation curve for Nusselt number valid for $Pr \geq .73$ and $Ra < 10^7$ is presented. At relatively low Rayleigh numbers the flow is caracterized by the development of double cells with flow up the center and down the sidewalls. However it was found that the increase of the Rayleigh number leads to the development of strong secondary circulation on the axis of symmetry of the cavity near the top wall. Thus, as the Rayleigh number is increased the secondary cells grow in size. The effects of the secondary cells on the temperature fields and heat transfer coefficients are discussed. Most results are obtained in the case of a square cavity ($E = 2$) but the influence of the aspect ratio of the cavity is also studied for $E = 1$ and 4.

NOTATION

b	enclosure width
C	wall constant cooling rate
C_p	specific heat at constant pressure
E	aspect ratio of the half cavity, h/b
$\vec{g}$	gravitational vector
g	acceleration due to gravity in x direction
h	enclosure height
k	thermal conductivity of fluid
N	dimensionless coordinate normal to a boundary
N_p	number of horizontal grid spaces
M_p	number of vertical grid spaces
Nu	Nusselt number, Eq.(18)
p	pressure
p'	dynamic pressure, Eq.(5)
Pr	Prandtl number, ν/α
q	local wall heat flux by unit area
Q	dimensionless average wall heat flux by unit area
Ra	Rayleigh number, $gb^3\beta\ \Delta T/\nu\alpha$
Ra'	modified Rayleigh number, Eq. (22)
Ra_{cr}	critical Rayleigh number separating the first and second modes of convection
T	temperature of fluid
ΔT	characteristic temperature difference, b^2C/α
t	time
u,v	velocities in x and y directions
U,V	dimensionless velocities in X and Y directions

$\vec{\omega}$ vector velocity

x,y cartesian coordinates

X,Y dimensionless cartesian coordinates

Greek symbols

α thermal diffusivity

β volumetric coefficient of expansion with temperature

ν kinematic viscosity

ρ density

ρ_o density at T_o

ΔT characteristic temperature difference, $b^2 C/\alpha$

τ dimensionless time (Fourier number), $\alpha t/b^2$

Φ_T, Φ_L, Φ_B dimensionless average heat flux at the top wall, side wall and bottom wall respectively

Φ_{av} dimensionless wall heat flux averaged over the boundaries of the entire cavity, Eqs. 16 and 17

ψ stream function

Ψ dimensionless stream function

ω vorticity

Ω dimensionless vorticity

θ dimensionless temperature, $(T - T_w)/\Delta T$

θ_c dimensionless temperature at the centre of the cavity

θ_{max} dimensionless maximum temperature

Superscripts

*	refers to pure conduction
-	refers to mixed mean temperature
$\sim$	refers to a value averaged over a given boundary

Subscripts

w	refers to wall condition
i	refers to initial condition
c	refers to the center of the cavity

Operators

$$\tilde{\nabla} = = \vec{i}(\partial/\partial x) + \vec{j}(\partial/\partial y)$$

$$\tilde{\nabla}^2 = (\partial^2/\partial x^2) + (\partial^2/\partial y^2)$$

$$\nabla^2 = (\partial^2/\partial X^2) + (\partial^2/\partial Y^2)$$

$$\frac{D}{Dt} = (\partial/\partial t) + u(\partial/\partial x) + v(\partial/\partial y)$$

$$\frac{D}{D\tau} = (\partial/\partial \tau) + U(\partial/\partial X) + V(\partial/\partial Y)$$

1. INTRODUCTION

The study of natural convection in enclosures is of importance in many industrial and geophysical problems [1]. Such problems may vary from the circulation in a vessel of liquid in which a crystal is being grown to the convective heat loss from a flat plate solar collector. Other problems include the natural convection cooling of nuclear fuel in shipping flasks [2] and the energy distribution in a geothermal liquid-dominated reservoir [3].

Analyses of the heat transfer due to natural convection in enclosures have received considerable attention since the 1960's. This is due to the remarkable development of the electronic computer allowing to economically evaluate the temperature and flow fields inside these enclosures. Particular attention has been directed in the past toward the study of rectangular cavities under the condition of isothermal vertical walls at different temperatures and under constant heat flux conditions. These systems were seen in an insulation double window. The calculated results obtained recently by several workers [4-9] agree with the experimental results. Reference [10] contains a comprehensive bibliography on this subject.

Natural convection with heat and mass transfer in a cavity whose walls are maintained at a uniform temperature which change at a steady rate, has received little attention in the litterature. Quack [11] , using a perturbation method, has studied the transient natural convection in long horizontal cylinders with a uniform initial fluid temperature and a linear variation of wall temperature. However the resulting perturbation solution is valid only for very low Rayleigh number regime ($Ra < 1.5 \times 10^3$) which

is not important practically. An interferometric investigation of convective heat transfer in a horizontal fluid cylinder with wall temperature increasing at a uniform rate has been performed by Deaver and Eckert [12]. Although the phenomenon is a transient one, a quasi-steady state develops if the heating rate is held constant long enough. Thus a correlation equation for Nusselt number in terms of Rayleigh number, valid for $Ra > 5 \times 10^5$, was obtained by these authors. More recently the transient natural convection in horizontal cylinder with constant cooling rate was approached by a numerical method by Takeuchi and Cheng [13] . For quasi-steady state, a generalized correlation equation for Nusselt number valid for $Pr \geq 0.7$ and $Ra \leq 10^7$ was developed.

The purpose of the present investigation is to study numerically the transient two-dimensional laminar convection and the heat transfer occuring in an enclosed rectangular cavity with wall temperature decreasing at a constant rate. The cooling process is supposed to be maintained long enough so that a quasi-steady state may be approached for which local temperature gradients, velocities, and other parameters are very nearly independent of time. If thermophysical properties are assumed constant, the equations describing this problem are identical with those for a fluid with uniform heat sources in a rectangular cavity whose walls are held at a constant uniform temperature. Thus the results of this study should apply as well to the uniform heat source problem.

2. MATHEMATICAL FORMULATION

Consider a cavity of width 2b and height h, shown schematically in Fig. 1, which contains a newtonian fluid. The aspect ratio of the half cavity is denoted by $E = h/b$. The fluid is initially motionless and at a uniform temperature T_i . At time $t = 0$ it is assumed that the cavity is subjected to a linear wall temperature decreasing with time as $T_w = T_i - Ct$. The problem is to find the subsequent velocities and temperatures as function of time and position inside the cavity and the rate of heat transfer across the enclosure as a function of time. A final steady state solution, if such exists, would be of particular interest. The motion in the fluid will be laminar provided the Rayleigh number based on cavity height is less than about 10^8 [5,6] .

For natural convection flows with small density changes it is common to make the Boussinesq approximation [14] , i.e., to assume that the effect of temperature on density is confined to the body force term of the momentum equation and that otherwise the thermodynamic and transport properties of the fluid are independent of temperature and pressure. This implies that the fluid is essentially incompressible, and that its equation of state is

$$\rho = \rho_o [1 - \beta(T - T_o)] \qquad (1)$$

where ρ, β and T denote respectively the density, volumetric expansion coefficient and temperature of the fluid, and the subscript denotes some reference state. Further, making the reasonable assumption that viscous dissipation is negligible , the fundamental equations are:

$$\frac{D\vec{\omega}}{Dt} = -\frac{\nabla p'}{\rho_o} + \nu \tilde{\nabla}^2\vec{\omega} + \begin{pmatrix} -g\beta(T-T_o) \\ 0 \end{pmatrix} \tag{2}$$

$$\frac{DT}{Dt} = \alpha \tilde{\nabla}^2 T \tag{3}$$

$$\tilde{\nabla}.\vec{\omega} = 0 \tag{4}$$

where $\vec{\omega} = \vec{i}\, u + \vec{j}\, v$ is the vector velocity field, α and ν are respectively the thermal diffusivity and kinematic viscosity.

In Eq.(2), the gravity vector has been taken to be in the x-direction as indicated in Fig. 1 and the pressure to be represented by a dynamic plus a static term such that:

$$\tilde{\nabla} p \equiv \tilde{\nabla} p' + \rho_o \vec{g} \tag{5}$$

The initial and boundary conditions appropriate to the present problem are:

$t = 0$	$u = v = 0$	$T = T_i$	
$x = 0$	$u = v = 0$	$T = T_w$	
$x = h$	$u = v = 0$	$T = T_w$	(6)
$y = 0$	$\frac{\partial u}{\partial y} = v = 0$	$\frac{\partial T}{\partial y} = 0$	
$y = b$	$u = v = 0$	$T = T_w$	

Furthermore, the dimensionless variables as shown in Eq.(7) are introduced and the dimensionless stream function Ψ and vorticity Ω are defined as Eqs. (8) and (9) respectively. After some manipulations the fundamental equations are written as Eqs. (8) - (11).

$$\tau = \frac{\alpha t}{b^2} \qquad X = \frac{x}{b} \qquad Y = \frac{y}{b}$$

$$\Omega = \frac{\omega b^2}{\alpha} \qquad U = \frac{ub}{\alpha} \qquad V = \frac{vb}{\alpha}$$

$$\Psi = \frac{\psi}{\alpha} \qquad \theta = \frac{T - T_w}{\Delta T} \qquad \Delta T = \frac{b^2 C}{\alpha} \tag{7}$$

$$Ra = (g\beta b^3 \Delta T)/\nu\alpha) \qquad Pr = \nu/\alpha$$

All other symbols are defined in the nomenclature.

$$U = \frac{\partial \Psi}{\partial Y} \quad , \quad V = - \frac{\partial \Psi}{\partial X} \tag{8}$$

$$\Omega = (\frac{\partial U}{\partial Y} - \frac{\partial V}{\partial X}) = - \nabla^2 \Psi \tag{9}$$

$$\frac{D\Omega}{D\tau} = Ra\ Pr \frac{\partial \theta}{\partial Y} + Pr\ \nabla^2 \Omega \tag{10}$$

$$\frac{D\theta}{D\tau} = \nabla^2 \theta + 1 \tag{11}$$

The inital and boundary conditions become Eq. (12)

$$\begin{aligned}
&\tau = 0 && \Psi = U = V = \Omega = \theta = 0 \\
&X = 0 && \Psi = U = V = \theta = 0 \\
&X = E && \Psi = U = V = \theta = 0 \\
&Y = 0 && \Psi = \Omega = V = \partial U/\partial Y = \partial\theta/\partial Y = 0 \\
&Y = 1 && \Psi = U = V = \theta = 0
\end{aligned} \tag{12}$$

It is noted in Eq. (7) that the characteristic temperature difference ΔT used in the Rayleigh number Ra is based on the constant wall cooling rate C. It is also observed that the dimensionless time $\tau = (\alpha t/b^2)$ is similar in form to Fourier number in unsteady heat conduction.

It should be mentioned at this stage that the unity ($b^2C\Delta T/\alpha = 1$) appearing on the right hand side of the energy equation, Eq. (11), can be regarded as a uniform heat source term. In fact the present problem with a wall temperature varying linearly with time as $T_w = T_i - Ct$ is equivalent to the transient natural convection heat transfer between a fluid with uniform internal heat sources of strength per unit time and volume $\rho C\ C_p$ and a cavity with constant wall temperature. It is noted that the solution of the governing equations with $C < 0$ corresponds to the transient natural convection for the case of constant heating rate. Finally it is observed in Eq. (12) that use has been made of the symmetry of the present problem with respect to a vertical plane passing through $Y = 0$ (see Fig. 1). With the boundary conditions specified in Eq. (12), solution for the stream function and temperature field exhibit the following symmetry:

$$\begin{aligned} \Psi(X,Y) &= \Psi(X,-Y) \\ \theta(X,Y) &= \theta(X,-Y) \end{aligned} \qquad (13)$$

which will be utilized to reduce numerical calculations.

In view of the complex nature of the governing equations, i.e. second order simultaneous partial differential equations of the parabolic and elliptic type respectively, a numerical solution appears to be the only practical approach for the present problem. In this numerical solution, the heat transfer, which is of practical interest, will be evaluated at the boundaries. The local heat flux q across a given boundary at any time t can be computed by considering the wall temperature gradient. The dimensionless local heat flux $Q = (qb)/(k\ \Delta T)$ is then given as:

$$Q = - \left(\frac{\partial \theta}{\partial N}\right)_{N=0} \tag{14}$$

where N is the dimensionless normal to the boundary.

Integrating Eq.(14) over the top boundary will give the dimensionless average heat flux Φ_T as:

$$\Phi_T = \frac{\tilde{q}_T \, b}{k \, \Delta T} = \int_0^1 \left(- \frac{\partial \theta}{\partial X}\right)_{X=E} dY \tag{15}$$

where $\tilde{q}_T$ is the average heat flux relative to the top boundary. Similar results may be obtained for the side and bottom boundaries.

The dimensionless average heat flux through the walls of the entire cavity is then given, in terms of the wall temperature gradients, as:

$$\Phi_{av} = \frac{1}{(2+E)} \left[\int_0^1 \left(\frac{\partial \theta}{\partial X}\right)_{X=0} dY + \int_0^E \left(- \frac{\partial \theta}{\partial Y}\right)_{Y=1} dX + \int_0^1 \left(- \frac{\partial \theta}{\partial X}\right)_{X=E} dY \right] \tag{16}$$

Furthermore it may be shown that Φ_{av} can also be computed by the following expression:

$$\Phi_{av} = \frac{E}{2+E} \left[1 + \int_0^E \int_0^1 \left(- \frac{\partial \theta}{\partial \tau}\right) dX \, dY \right] \tag{17}$$

in which the time rate of change of fluid temperature has been considered.

The Nusselt number based on the temperature difference between mixed mean temperature $\bar{T}$ and wall temperature T_w is defined as :

$$Nu = \frac{2b}{k} \frac{(\tilde{q}_T + \tilde{q}_B + \tilde{q}_L)}{(\bar{T} - T_w)} = \frac{2\Phi_{av}}{\bar{\theta}} \tag{18}$$

where $\bar{\theta} = \frac{1}{E} \int_0^E \int_0^1 \theta \, dX \, dY$

3. NUMERICAL SOLUTION OF THE GOVERNING EQUATIONS

3.1 Finite difference procedure

The coupled transport and energy equations (10) and (11) are quasi-linear, second-order partial differential equations of the parabolic type and such numerical methods as standard explicit method, alterning direction implicit method, Dufort-Frankel method and others may be applicable. In this study a two-dimensional alternating direction (A.D.I.) procedure is employed and the computational method involved differs slightly from that used by Mallison and de Vahl Davis [9]. The first and second derivative were approximated by central differences and the time derivatives by a first order forward difference. The finite difference form of the equations were written in conservative form for the advective terms in order to preserve the transportive property (Roache [15]). Applying the A.D.I. method to Eqs. (10) and (11) produces first-order algebric equations with a coefficient matrix of three-diagonal components. The unknowns are solved by line in the X and Y directions. The A.D.I. technique has the advantage over explicit methods that it is numerically more stable and hence allows the use of a larger time step $\Delta\tau$. However it has the disadvantage that each iteration requires more computations than does an iteration with the explicit techniques.

The elliptic equation for the stream function, Eq. (9) was solved by the method of successive over-relaxation (S.O.R.) for the new field which is then used to obtain the velocities from Eq. (8) and the wall vorticity (which requires the velocity boundary conditions).

Boundary conditions on Ψ and θ are applied in the usual manner, using central differences whenever possible and image points for derivative conditions. Exact boundary conditions for Ω are not known in the present problem. However, approximate values of Ω on the boundaries can be obtained from the most recent estimates of either Ψ using Eq. (9), or from U and V, using Eq. (8). The first method was utilized by both Wilkes and Churchill [7] and Gossman et al [16] , while Aziz and Hellums [17] used the second. In the present study the second method was used since it was found, from our numerical experimentations, that in general it yielded more stable results. Furthermore the second method has the advantage that any instability associated with it can be eliminated by using the mean of the distribution of Ω at the wall from two successive iterations (Newell and Schmidt [10]). It should be mentionned for completeness that the present technique produces unstable results for large Rayleigh numbers. As discussed in reference [18] this probably arises from the fact that the implicit computation of the new interior vorticities supposes that the old boundary vorticities still hold good at the end of the time increment. The boundary vorticities themselves are eventually advanced on the basis of Taylor's series expansions for the flow field at one or two points adjacent to the boundary. The resulting slight inconsistency between the interior and boundary vorticities could be overcome at the expense of iterating several times over each time step. Such a procedure has not been carried out in the present calculations.

3.2 Effect of mesh size

The determination of an acceptable mesh size is of prime importance since it is well known that it introduces errors that depend explicitely on the grid spacing. To minimize this truncation error, it is desirable to use the smallest grid spacing possible throughout the domain of integration. However, since the computational time increases markedly as the number of grid points is increased, one must reach a compromise between the accuracy of the solution and the computation time necessary to reach the solution.

Square cavities have received thorough consideration in regard with the effect of grid spacing on the numerical solution. For instance, Elder [6] found that solutions obtained with an 11x11 grid were qualitatively acceptable, that a marked improvement occured when the mesh size was halved to 21x21 , but that little further change resulted when a finer mesh was used. Similarly it was found by Wilkes [18] that the use of a 10x10 grid gives results remarkably close to that of a 20x20 grid, a 15% difference in the heat transfer at walls between the two being however observed. This difference was attributed to the inherent difficulty in estimating the temperature gradient on the wall from values of temperature at grid extending one side of the wall only. As noticed by Rubel and Landis [19] indications that a given mesh size will become inadequate as Ra increases are most easily given by the appearence of local temperature peak and by the unexpected rise of the average heat transfer. The same type of problem was also observed in the present study when the time increament was choosen too high. A more insidious problem is the possible

error in the flow configuration where the truncations errors introduced by coarse mesh size can lead to spurious multiple cells.

These different results suggest that a 20x20 grid is the most adequate mesh for a satisfactory determination of both flow and heat transfer. Due to the symmetry of the present problem the numerical domain for a square cavity is in fact a rectangular space with h=2b. A mesh size of 20x10 was thus utilized in most of the calculations presented in this study excepted for the cases involving relatively high Rayleigh numbers for which a 30x15 grid was used.

3.3 Computational requirements

All calculations were performed on a IBM 360/70 computer where for a 20x10 mesh the average time for a single step of Eq. (9), the most time-consuming operation, was about 0.12 s. The test for convergence of iteration involved the calculation of the absolute value of the maximum relative difference between two consecutives iterations, and comparing it with a prescribed constant. The condition may be stated as :

$$\Sigma \left| \psi_{i,j}^{n+1} - \psi_{i,j}^{n} \right| \Big/ \Sigma \left| \psi_{i,j}^{n+1} \right| \leqslant \epsilon \qquad (19)$$

in which $\psi_{i,j}^{n}$ denotes the approximation at the n th iteration to the stream function at a point, $\psi_{i,j}^{n+1}$ a further approximation and ϵ some prescribed value.

It is obvious that the value of ϵ must depend upon the numerical scheme used and the round off error. By numerical experiments on the com-

puter it was established that ϵ must be 10^{-4} to 10^{-5}, depending on the parameters of the problem. In most of the calculations presented in this paper it was found that the number of iterations required decreases rapidly from about 30 immediatly after the start of the cooling to 1-3 for most other time steps.

It was observed that a larger discrete time step could be used for the integration of the temperature equation than for the vorticity equation. Hence, to reduce the computation time require to reach the final solution, a different time step was used in each equation. It was also noticed that during the initial cooling period, a small time step is required for accurate solution since the variation of the temperature field with time is large. However, with small $\Delta\tau$ the number of steps required to reach a quasi-steady state was found to be impractically large. Consequently, a continually increasing time step was used to increase the computational efficiency.

To expedite plotting of the results, an auxilliary computer program was written to locate points lying on specified isotherms and streamlines by linear interpolation of the computed values at the grid points. As mentioned earlier the problem under consideration is symmetrical and it was found advantageous to reproduce the computer results at a given time on a single graph with the flow pattern on the right half of the cavity and the isotherms on the left half. All graphs were performed on the Ecole Polytechnique CALCOMP 563 automatic plotter.

The total time steps necessary to solve a typical case ranged from about 1100 to 1500 and the corresponding computing time on an IBM 360/70 computer was from 8 to 12 minutes approximately depending on the parametric values of the case treated.

4. RESULTS AND DISCUSSION

Numerical results obtained in the present study have revealed that, depending on the Rayleigh number, two different modes of convection may be observed inside the cavity. For relatively low Rayleigh numbers, the flow pattern develops into a standard conterrotating vortex pair. However, when the Rayleigh number is increased sufficiently, the previous flow configuration referred in this study as the first mode of convection, is modified by the superposition of two additional secondary vortices symmetrically located near the upper boundary. The resulting more complex convective circulation, termed as second mode of convection, appears to be a characteristic of the particular geometry and boundary conditions considered in this investigation.

As discussed previously, the present problem is basically transient. However, if the cooling process is maintained long enough, a quasi-steady state is reached. The first part of discussion describes the time evolution of the flow and temperature fields and related heat transfer for the two possible modes of convection. Quasi-steady solutions are of great interest in themselves and are presented in the second part.

4.1 Time-dependent Results

The calculated isotherm and streamline fields for Pr = 7.3, Ra = 5×10^4 and Ra = 3×10^5 at four different times steps between the initial conditions and the quasi-steady state situation are shown in Figs. 2 and 4. They illustrate respectively the establishment of the first and second mode of convection. The corresponding transient velocity profiles along X = 1 (a), temperature profiles along Y = 0 (b) and X = 1 (c) and average heat flux distributions on each wall of the cavity (d) are presented in Figs. 3 and 5.

The development of the first mode of convection ($Ra = 5 \times 10^4$) is depicted in Figs. 2 and 3. The resulting flow and isotherm patterns are quite similar to those obtained experimentally by Deaver and Eckert [12] and numerically by Takeuchi and Cheng [13]. This initial stage of cooling is characterized by a pure conduction heat transfer as indicated by the isotherms of Fig. 2a. Due to the symmetry with respect to the vertical plane $Y = 0$, a pair of counterrotating vortices is formed. Fig. 2a only shows the right clockwise vortex. As the cooling progresses, the vortex gradually increases its strength (Fig. 2b). The convective motion progressively stratifies the core region and the isotherm configuration becomes closely spaced near the top wall but sparely spaced near the bottom one, indicating respectively large and poor heat transfer on those boundaries (Figs. 2c and 3d). Fig. 2d shows the stabilized pattern of streamline and isotherms corresponding to the quasi-steady state situation. The vortex center has moved close to the lateral boundary and its strength has decreased to some extent.

The development of the second mode of convection ($Ra = 3 \times 10^5$) is illustrated in Figs. 4 and 5. At the initial stage of the cooling, the temperature and flow fields are quite similar to those observed for the first mode of convection. This is shown in Fig. 4a, where a pair of counterrotating vortices develops. However, due to the higher Rayleigh number involved in the present case, there is a strong tendency for the vortex center to move very close to the side boundary (Fig. 4b). The velocity profile tends to be of the boundary layer type, as illustrated in Fig. 5a while the fluid in the upper central region of the cavity becomes almost stagnant. Furthermore, the fluid in this region is unstable because of the top heavy situation resulting from the particular temperature field prevailing near the top wall.

The induced density field combined to the existing flow motion gives rise to an additional pair of secondary vortices symmetrically located on the axis of symmetry, near the upper boundary (Fig. 4b). The occurence of this secondary motion presents some similarity with the start of the inversion process studied in [20] for the case of water cooled through $4^{o}C$. With time progression the additional vortex pair increases its strength as it may be seen by comparing Figs. 4b and 4c. The quasi-steady state situation is depicted in Fig. 4d in which the secondary vortex has reached its equilibrium intensity. It results from this particular flow pattern that the relatively cold fluid penetrates the core region not only from the bottom but also from the top of the cavity. This motion perturbates greatly the isotherm field in the centre upper region (compare Figs. 4d and 2d). Furthermore the second mode of convection allows the warmer core fluid to reach the region near the top boundary by two paths instead of one. The noticeable bump characterizing the heat transfer Φ_T in Fig. 5d corresponds to the occurence of the secondary motion. It was observed from numerical results that this secondary motion develops very rapidly, giving rise to this sudden increase of Φ_T.

It is interesting to note that for the case of the cooling of a circular fluid cylinder [12, 13] no comparable secondary motion has been reported. It is true that multicellular flows have been observed both experimentally and theoretically in the past. However, those secondary motions were rather related either to the high aspect ratio of the cavity [6] or to low Prandtl number effects [22]. In fact the second mode of convection observed in this study results essentially from the interaction between the zone of instability located near the top boundary and the flow field induced by the side wall. This situation arises from the particular geometry and thermal boundary conditions involved in the actual problem. The origin of

the secondary motion depicted in the present investigation appears more closely related to the multicellular flow arising from instabilities such as those studied by Samuel and Churchill [21].

In order to study the effect of the Prandtl number the quasi-steady state situations of Fig. 2d and 4d were computed for a Prandtl number of .73. Results are shown on Figs. 6a and 6b. It is seen that for a given Rayleigh number a decrease of Pr 1^{o} lowers the position of the vortices center, 2^{o} promotes the occurence of the secondary motion (compare Figs. 2d and 6a), and 3^{o} increases the size of the secondary vortex when it is present.

The influence of the aspect ratio E on the flow configuration is illustrated on Figs. 7a and 7b for E = 4 and 1 respectively. Qualitatively the general features of the flow and temperature field remain similar to those obtained with E = 2. However, in the case of the shallow cavity the secondary motion is enhanced. This is due to the fact that, with decreasing E, the instability zone related to the vertical density gradient near the upper horizontal boundary becomes more important whereas the stabilizing driving force generated by the horizontal density gradient near the vertical wall is reduced.

The relationship at different Ra between the dimensionless wall heat flux averaged over the boundaries of the entire cavity Φ_{av} and the dimensionless time τ is shown in Fig. 8 for Pr = .73 and 7.3. It is clear from the results that the heat transfer mechanism involved in the present problem is caracterized by three distinct regimes namely pure conduction, intermediate and asymptotic regimes. When the asymptotic regime, or quasi-steady state, is reached, the cooling rate inside the cavity becomes equal to the wall cooling rate C. The rate of heat flow per unit length of cavity

is then $2\ E\ b^2\ \rho\ C_p$. Substituting $\partial\theta/\partial\tau = 0$ in Eq. (17) gives the value of the average heat flux Φ_{av} as:

$$\Phi_{av} = E/(2 + E) \tag{20}$$

Thus, for a square cavity, $\Phi_{av} = .5$ for the quasi-steady state regime and all the curves on Fig. 8 tend towards this value independently of the Rayleigh number. Fig. 8 indicates not only the time necessary to reach a quasi-steady state for a particular Ra and Pr, but also the onset of natural convection effect as given by the time τ at which a deviation from the pure conduction curve occurs. It is noticed of Fig. 8 that for the higher Rayleigh numbers oscillations are present in some of the curves and the computations are terminated before reaching the quasi-steady state. These oscillations might well be an indication of the occurence of turbulence since, for these high Rayleigh number values, this latter is expected to take place. However, in order to reproduce properly the strong transients associated with those oscillations, very small time increments would have been necessary, rendering rapidly prohibitive the computing time required to reach the quasi-steady state. For this reason no intensive study of these oscillations was carried on. Nevertheless it is worth to notice that the instabilities are more accentuated for Pr = .73 than Pr = 7.3. This result is understandable owing to the fact that at large Pr the non linear inertia term becomes negligible in the vorticity equation, thereby attenuating the instabilities which characteristically arise from non linearity.

The time required to reach a quasi-steady state is of practical importance and the results obtained with a square cavity for Pr = .73, 7.3 and 73. are presented in Fig. 9. In this figure the quasi-steady state is assumed to be reached when $\Phi_{av} = .485$, i.e. 97 percent of the asymptotic

value $\Phi_{av} = .5$. The resulting curve, expressed as a function of Ra, is observed to be independent of the Prandtl number. Furthermore this curve indicates that for $Ra = 10^7$ the time required to reach a quasi-steady state is only about one-seventh of that for the pure conduction case. Finally it is observed that the occurence of the second mode of convection has a noticeable effect on the slope of this curve. Fig. 9 also shows the time τ when 2 percent deviation from the pure conduction case occurs, this time being an indication of the onset of natural convection effects. A distinct curve is obtained for Pr = .73, indicating a Prandtl effect associated with the transient aspect of the solution.

4.2 Quasi-steady State Results

The exact solution of the steady heat conduction inside an infinite rectangular cavity whose walls are kept at constant temperature and with an internal heat production at a constant rate is well known [23]. For such a situation the Nusselt number is given by:

$$Nu = 2\left(\frac{E}{2+E}\right) \frac{1}{\overline{\theta^*}} \qquad (21)$$

where

$$\overline{\theta^*} = \int_0^E \int_0^1 \left[\frac{(1-X^2)}{2} - \frac{16}{\pi^3} \sum_{n=0}^{\infty} \frac{(-1)^n \cos(2n+1)\pi\, X/2 \cosh(2n+1)Y/2}{(2n+1)^3 \cosh(2n+1)\pi\, E/2} \right] dX\, dY$$

Evaluating Eq. (21) for cavities with aspect ratio of E = 1, 2 and 4 gives Nusselt numbers of 11.70, 7.12 and 5.85 respectively. As a preliminary test to establish the overall consistency of the numerical results obtained in the present study, the program was run for the above mentionned

conditions. With a 30 X 15 grid, nusselt numbers of 11.71, 7.13 and 5.87 were obtained respectively.

Quasi-steady state results concerning the velocity and temperature profiles, wall heat flux averaged over the boundaries Φ_T, Φ_L and Φ_B and the temperatures θ_c, θ_{max} and $\overline{\theta}$, are presented in Figs. 10 and 11 at different Ra. On all thoses graphs, the pure conduction solution is given for comparison purpose. In particular the pure conduction temperatures $\theta_c^* = \theta_{max}^* = .295$ and $\overline{\theta}^* = 0.140$, evaluated from [23], are represented by dash lines on Figs. 10d and 11d. Since it is well known that, for moderate Rayleigh numbers, the solution are practically independent of the Prandtl number, provided $Pr > 1$, the results for Pr = 7.3 and 73 are presented on the same graphs, Figs. 10, whereas those for Pr = .73, on Figs. 11.

4.2.1 Rayleigh effect

Figs. 10 show that when Ra is low, the velocities are small and the temperature profiles and heat transfer results deviate only slightly from the pure conduction case. With increasing Rayleigh, the convective motion is amplified (see Fig. 10a) and consequently Φ_T increases whereas Φ_B decreases, as it can be noticed on Fig. 10c. The value $\Phi_{av} = .5$ is represented by a dashed line on that figure. The behaviour of the temperature inside the cavity as a function of Rayleigh is depicted on Fig. 10d. It is seen that an increase of the Rayleigh number promotes the convective heat transfer, thus reducing the difference of temperature between a given interior point of the cavity and the boundary.

For $Ra \geqslant Ra_{cr} \approx 80{,}000$, the second mode of convection is set up. Corresponding numerical results are represented by blackened symbols on Figs. 10c and 10d. It is noticed that the apparition of the additional

vortices abruptly enhances Φ_T and reduces Φ_L, Φ_{av} remaining constant. As the Rayleigh number increases further, the nature of the flow becomes more and more of the boundary layer type (see Fig. 10a). Furthermore Fig. 10c indicates that for $Ra > \sim 2 \times 10^5$, results obtained for the two different Pr produce distinct curves. A similar behaviour has been reported in [4].

4.2.2 Prandtl Effect

Figs. 11 show the results obtained for Pr = .73 and it is seen that the general trend is comparable to that discussed in Figs. 10. However a value of 6×10^4 is now obtained for Ra_{cr}, indicating that the second mode of convection occurs at lower Ra when Pr is reduced. Furthermore it is seen that the jumps in the curves for Φ_T, Φ_L, θ_{max}, θ_c and $\overline{\theta}$ are more pronounced.

The particular behaviour of the heat transfer and temperature curves near the critical Rayleigh number suggests a possible hysteresis effect. Numerical tests have been performed for Pr = 7.3 and .73, at Rayleigh numbers slightly below Ra_{cr}, using as initial conditions steady-state results obtained from a case involving the second mode of convection. Tests for Pr = 7.3 indicate no significant hysteresis effect. For Pr = .73, there has been some hysteresis effect detected over a very limited range of Rayleigh values, this effect vanishing completely at $Ra = 4 \times 10^4$.

4.2.3 Aspect ratio effects

The relationship between Nusselt number Nu and the modified Rayleigh number Ra' for the quasi-steady state is of practical interest and the results obtained for cavities with E = 1, 2 and 4. are presented in

Fig. 12. The relationship between the modified Rayleigh number Ra', based on the temperature difference between mixed mean temperature $\overline{T}$ and wall temperature T_w, and the Rayleigh number Ra is given by:

$$Ra' = \frac{g(2b)^3\beta}{\nu\alpha} \quad (\overline{T} - T_w) = 8\ \overline{\theta}\ Ra \qquad (22)$$

The limit values of Nu corresponding to the pure conduction case (i.e. $Ra' \to 0$), obtained from Eq. 21, are indicated on the graph for reference. It is seen from the curves that the pure conduction theory is valid for $Ra' <\sim 5 \times 10^2$ when $E = 4$ and $Ra' <\sim 5 \times 10^3$ when $E = 1$. Furthermore it may be observed that as Ra' increases, the three curves tend to collapse.

The relationship between $\overline{\theta}/\overline{\theta}^*$ and Ra for three different aspect ratios E is presented on Fig. 13. The ratio $\overline{\theta}/\overline{\theta}^*$ is a measure of the relative importance of heat transfer by convection as compared to that by conduction. Thus, for $\overline{\theta}/\overline{\theta}^* = 1$, heat transfer results from pure conduction only. For a given $\overline{\theta}/\overline{\theta}^*$, the importance of the unstable zone located near the top wall is amplified when the aspect ratio is decreased. The critical values of $\overline{\theta}/\overline{\theta}^*$ at which the second mode of convection occurs are identified on the graph for each curve plotted. It is seen that the critical value $\overline{\theta}/\overline{\theta}^* = .63$ corresponding to the smallest aspect ratio is the largest. This result indicates that the occurence of the second mode of convection is strongly related to the unstability zone.

5. CONCLUDING REMARKS

The natural convection of a fluid contained in a rectangular cavity, the wall of which is maintained at a temperature decreasing at a constant rate, has being study numerically for Prandtl numbers Pr = .73,

7.3 and 73., aspect ratio of the cavity E = 1, 2 and 4 and a range of Rayleigh numbers Ra = $10^2 \sim 10^8$. The results obtained in the present study may be summarized as follows:

i) A quasi-steady state regime is reached from initial conditions where the fluid is at rest and at a uniform temperature. The transient solution is characterized at the initial stage by pure conduction. Subsequently a developping regime occurs where motion is set up inside the cavity. At a sufficiently large time, velocities, flow patterns and temperature differences between the fluid and the wall tend to become constant with time. The effects of unsteady terms in the governing equation are then negligible and the quasi-steady state is reached.

ii) Depending mainly on Rayleigh number, two distinct modes of convection may develop inside the cavity. In the first mode, occuring at relatively low Rayleigh numbers, the flow field is characterized by a single pair of counterrotating vortices. For Rayleigh numbers beyond a critical value, a second mode appears in which an additional pair of counterrotating vortices, located near the top boundary is superposed to the basic flow of the first mode. This second mode was found to enhance the convective heat transfer near the top boundary.

iii) The influence of the aspect ratio of the cavity on the occurence of the second mode of convection has been studied for E = 1, 2 and 4. For a given intensity of convection, the importance of the unstable zone increases with a decreasing E, thus promoting the second mode.

iv) The effect of the Prandtl number on the present problem follows the trend already reported in past litterature. For $Pr > 1$ (7.3 and 73), the flow and temperature field and the resulting heat transfer was found to be almost independent of Pr except for very high values of the Rayleigh number. For $Pr < 1$ (.73), some effect of Pr was observed.

ACKOWLEDGMENTS

This work was supported by the National Research Council of Canada through grants NRC A-4197 and NRC A-9201. The authors wish to gratefully thank Ecole Polytechnique for providing necessary time on an IBM 360/79 computer.

REFERENCES

[1] Hess,C.F. and Miller, C.W., Int. J. Heat Mass Trans. 1979, 22, 421.

[2] Chan, A.M.C. and Banerjee, S., Trans. A.S.M.E. 1979, 101, 114.

[3] Ribando, R.J. and Torrance, R.E., A.S.M.E. paper 75-WA/HT-73, 1975, 1.

[4] De Vahl, Davis G., Int. J. Heat Mass Trans. 1968, 11, 1675.

[5] Eckert, E.R.G. and Carlson, W.O., Int. J. Heat Mass Trans. 1961, 2, 106.

[6] Elder, J.W., J. Fluid Mech., 1965, 26, 77.

[7] Wilkes, J.O. and Churchill, S.W., A.I. Ch. E.J. 1966, 12, 161.

[8] Fromm, J.E., Phys. Fluids 1965, 8, 1757.

[9] Mallison, G.D. and De Vahl, Davis G., J. Comp. Phys., 1973, 12, 435.

[10] Newell, M.E. and Schmidt, Trans. A.S.M.E. , 1970, C 92, 159.

[11] Quack, H., "Warme-und-Stoff"urbertragung, 1970, 3, 134.

[12] Deaver, F.K. and Eckert, E.R.G., Heat Transf. 1970, 4, Paper NC 1.1, Elsevier Publishing, Amsterdam.

[13] Takeuchi, M. and Cheng, K.C., "Warme-und-Stoff"ubertragung, 1976, 9, 215.

[14] Gray, D.D. and Giorgini, A., Int. J. Heat Mass Trans., 1976, 19, 545.

[15] Roache, P.J., Computational Fluid Dynamics. Hermosa Publishers, 1976.

[16] Gossman, A.D., Pun, W.N., Runchal, A.K., Spalding, D.B. and Worfshstein, Heat and Mass Transfer in Recirculating Flow. Academic Press, London, 1969.

[17] Aziz, K. and Hellums, J.D., Physics Fluids, 1967, 10 (2), 314.

[18] Wilkes, J.D., Ph.D. Thesis, University of Michigan, 1963.

[19] Rubel, A. and Landis, F., Supplement to Physics of Fluids, 1969, II, 208.

[20] Robillard, L. and Vasseur, P., ASME/AICHE National Heat Transfer Conference, Orlando, Florida, paper 80-HT-74, 1980.

[21] Samuel, R. and Churchill, S.T., A.J.Ch.E.J. 1967, 13, 1, 77.

[22] Charrier-Mojtabi, M.C., Mojtabi, A. and Caltagirone, J.P., Trans. A.S.M.E. 1979, 101, 171.

[23] Carlslaw, H.S. and Jaeger, J.C., Conduction of Heat in Solids, 2 nd Ed., Oxford Univ. Press, 1959.

LIST OF FIGURES

Fig. 1 Coordinate system and boundary conditions.

Fig. 2 Transient streamline and isotherm fields for $Pr = 7.3$, $Ra = 5x10^4$ and $E = 2$ at various time τ. The centerline and walls have value $\Psi = 0$. The values of Ψ_{max} and $\Delta\Psi$ are (a) $\Psi_{max} = .33$, $\Delta\Psi = .033$; (b) $\Psi_{max} = 6.9$, $\Delta\Psi = .69$; (c) $\Psi_{max} = 9.8$, $\Delta\Psi = .98$; (d) $\Psi_{max} = 9.0$, $\Delta\Psi = .90$.

Fig. 3 Transient velocity profiles along $X = 1$ (a) and temperature profiles along $Y = 0$ (b) and $X = 1$ (c) and average wall heat flux distribution (d) for $Pr = 7.3$, $Ra = 5x10^4$ and $E = 2$ at various times τ.

Fig. 4 Transient streamline and isotherm fields for $Pr = 7.3$, $Ra = 3x10^5$ and $E = 2$ at various times τ. The centerline and walls have value $\Psi = 0$. The values of Ψ_{max}, Ψ_{min} and $\Delta\Psi$ are (a) $\Psi_{max} = 19.0$, $\Delta\Psi = 1.90$; (b) $\Psi_{max} = 17.0$ $\Psi_{min} = -0.2$, $\Delta\Psi = 1.72$; (c) $\Psi_{max} = 17.0$, $\Psi_{min} = -2.2$, $\Delta\Psi = 1.87$; (d) $\Psi_{max} = 16.0$, $\Psi_{min} = -9.7$, $\Delta\Psi = 2.57$.

Fig. 5 Transient velocity profiles along $X = 1$ (a) and temperature profiles along $Y = 0$ (b) and $X = 1$ (c) and average wall heat flux distribution (d) for $Pr = 7.3$, $Ra = 3x10^5$ and $E = 2$ at various times τ.

Fig. 6 Quasi-steady state streamline and isotherm fields for $Pr = .73$ and $E = 2$. The centerline and walls have value $\Psi = 0$. The values of Ra, Ψ_{max}, Ψ_{min} and $\Delta\Psi$ are
(a) $Ra = 5x10^4$, $\Psi_{max} = 8.1$, $\Psi_{min} = -.02$, $\Delta\Psi = .81$;
(b) $Ra = 3x10^5$, $\Psi_{max} = 15.0$, $\Psi_{min} = -9.5$, $\Delta\Psi = 2.45$.

Fig. 7 Quasi-steady state streamline and isotherm fields for $Pr = 7.3$. The centerline and walls have value $\Psi = 0$. The values of Ra, E, Ψ_{max}, Ψ_{min} and $\Delta\Psi$ are
(a) $Ra = 7x10^4$, $E = 4$, $\Psi_{max} = 16.0$, $\Psi_{min} = -7.1$, $\Delta\Psi = 2.3$;
(b) $Ra = 3x10^6$, $E = 1$, $\Psi_{max} = 19.0$, $\Psi_{min} = -12$, $\Delta\Psi = 15.5$.

Fig. 8 Φ_{av} as a function of τ with Ra as a parameter for $Pr = .73$ and 7.3 .

Fig. 9 Onset of natural convection effects and time to reach quasi-steady state.

Fig. 10 Temperature profiles along $Y = 0$ (a) ; velocity profiles along $X = 1$ (b), average wall heat flux (c) and typical temperature (d) distributions as function of Ra , at quasi-steady state for $Pr = 7.3$ and 73.

Fig. 11 Temperature profiles along $Y = 0$ (a), velocity profiles along $X = 1$ (b), average wall heat flux (c) and typical temperature (d) distributions as function of Ra, at quasi-steady state for $Pr = .73$.

Fig. 12 Relationship between Nusselt number and modified Rayleigh number for the quasi-steady state.

Fig. 13 Relationship between $\bar{\theta}/\bar{\theta}^*$ and Ra for $E = 1$, 2 and 4.

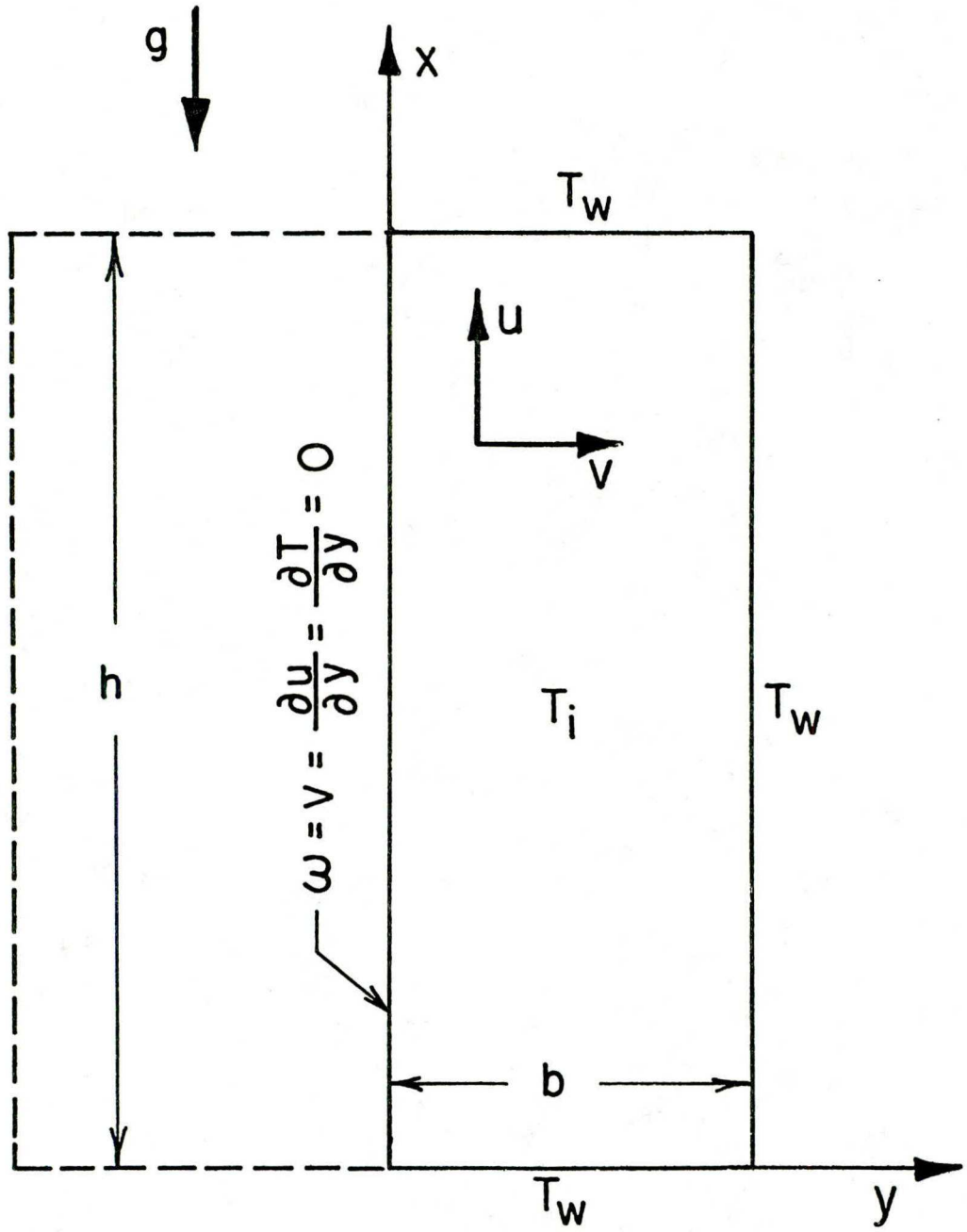

Fig. 1 Coordinate sytem and boundary conditions

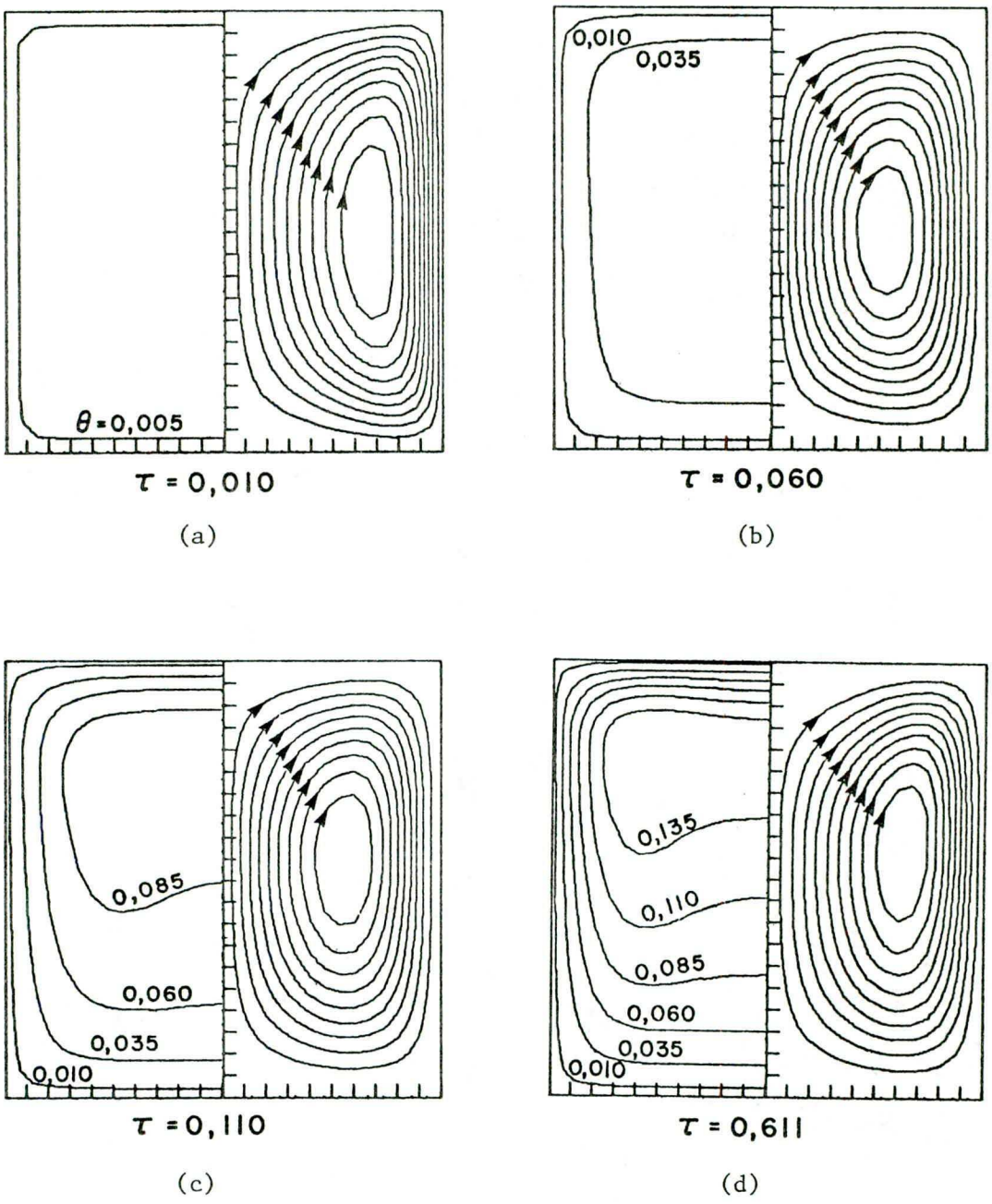

Fig. 2 Transient streamline and isotherm fields for $Pr = 7.3$, $Ra = 5 \times 10^4$ and $E = 2$ at various times τ. The centerline and walls have value $\Psi = 0$. The values of Ψ_{max} and $\Delta\Psi$ are (a) $\Psi_{max} = .33$, $\Delta\Psi = .033$; (b) $\Psi_{max} = 6.9$, $\Delta\Psi = .69$; (c) $\Psi_{max} = 9.8$, $\Delta\Psi = .98$; (d) $\Psi_{max} = 9.0$, $\Delta\Psi = .90$.

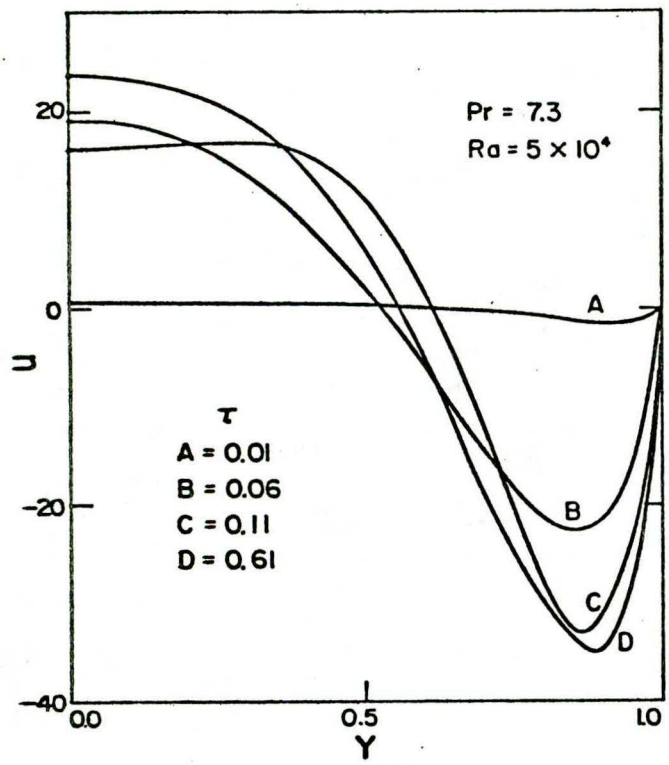

(a)

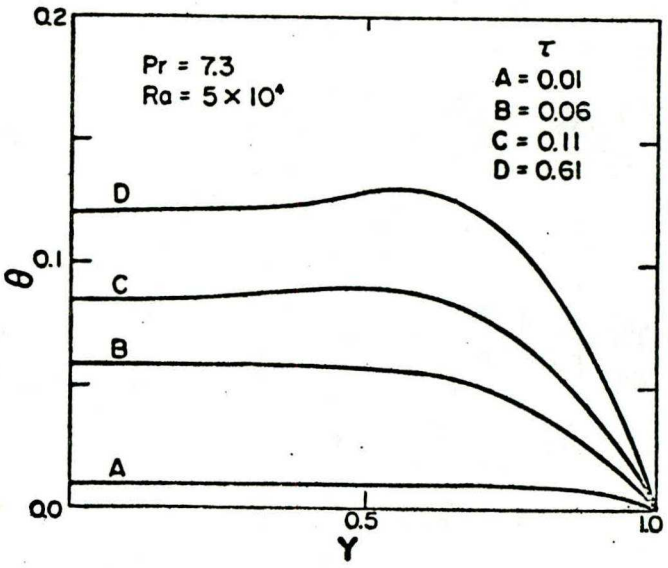

(c)

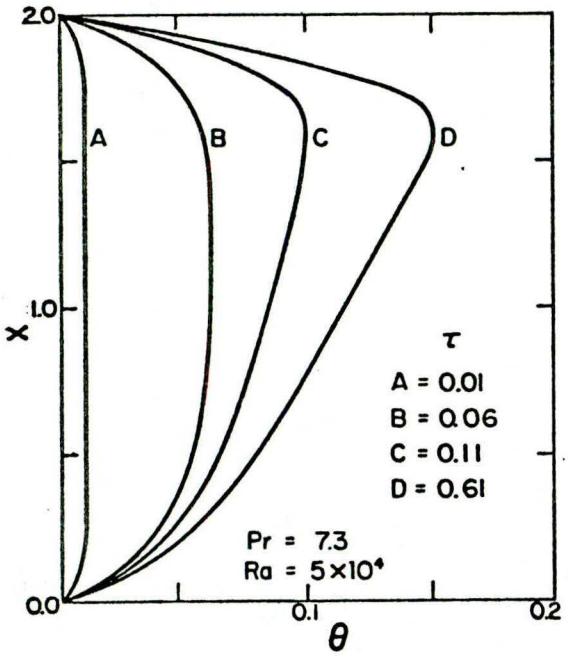

(b)

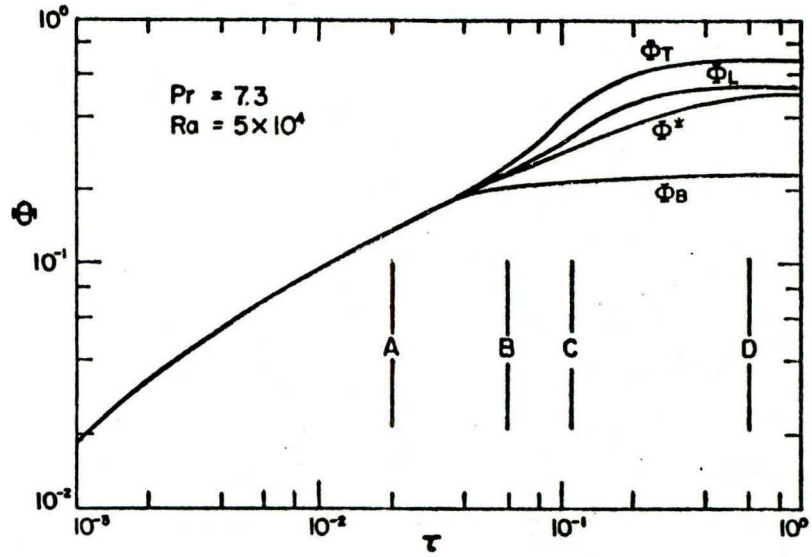

(d)

Fig. 3 Transient velocity profiles along X = 1 (a) and temperature profiles along Y = 0 (b) and X = 1 (c) and average wall heat flux distribution (d) for Pr = 7.3 , Ra = 5×10^4 and E = 2 at various times τ.

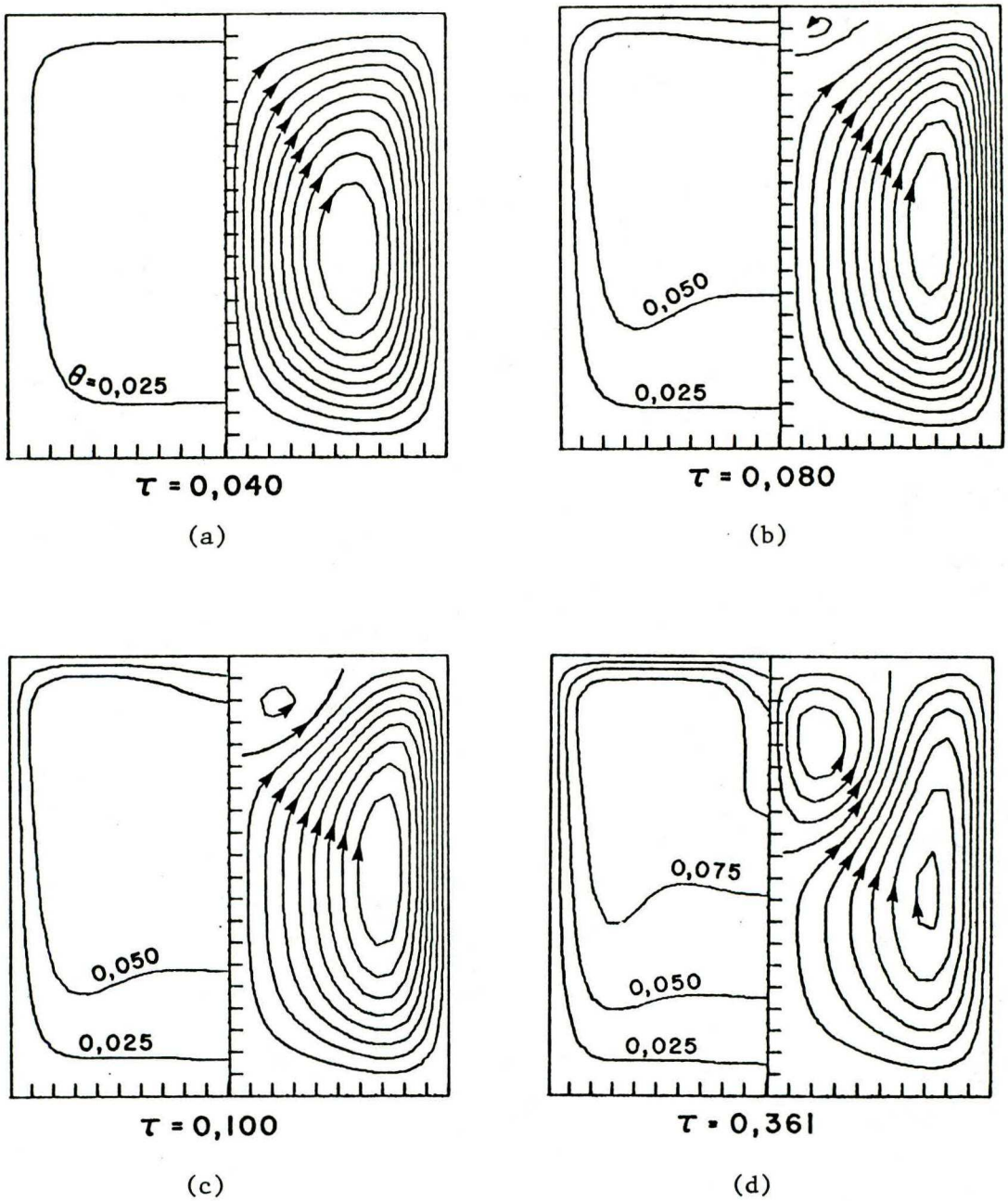

Fig. 4 Transient streamline and isotherm fields for $Pr = 7.3$, $Ra = 3 \times 10^5$ and $E = 2$ at various times τ. The centerline and walls have value $\Psi = 0$. The values of Ψ_{max}, Ψ_{min} and $\Delta\Psi$ are (a) $\Psi_{max} = 19.0$, $\Delta\Psi = 1.90$; (b) $\Psi_{max} = 17.0$ $\Psi_{min} = -0.2$, $\Delta\Psi = 1.72$; (c) $\Psi_{max} = 17.0$, $\Psi_{min} = -2.2$, $\Delta\Psi = 1.87$; (d) $\Psi_{max} = 16.0$, $\Psi_{min} = -9.7$, $\Delta\Psi = 2.57$.

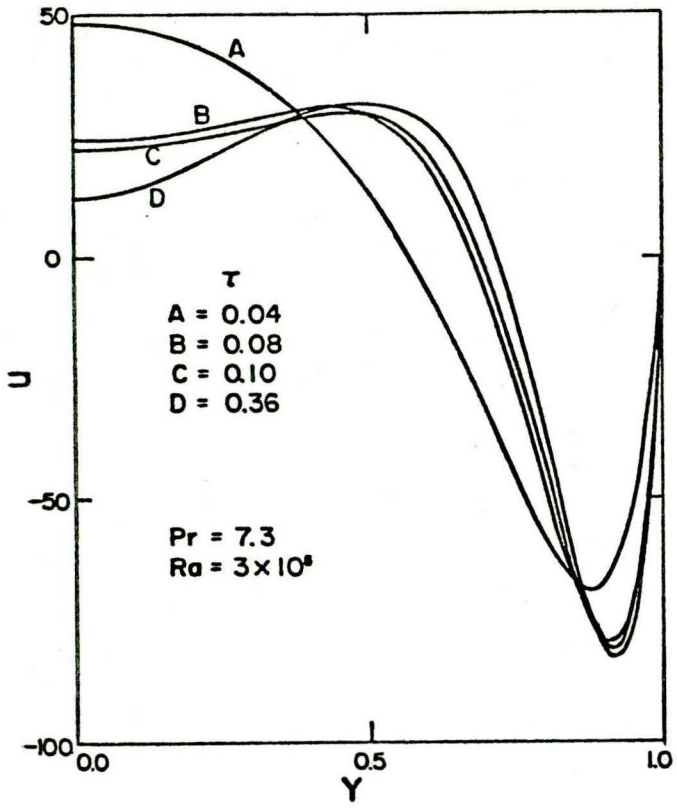

(a)

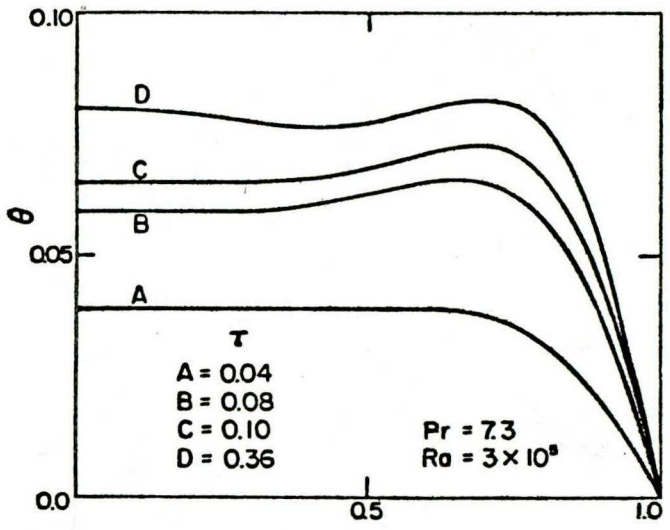

(c)

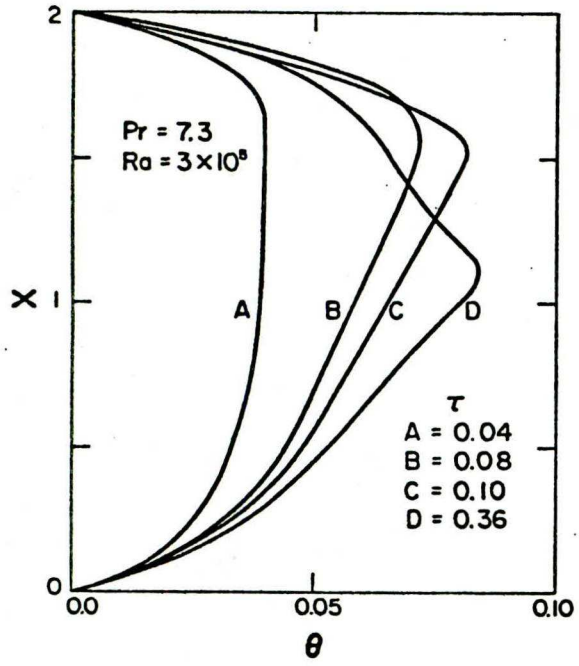

(b)

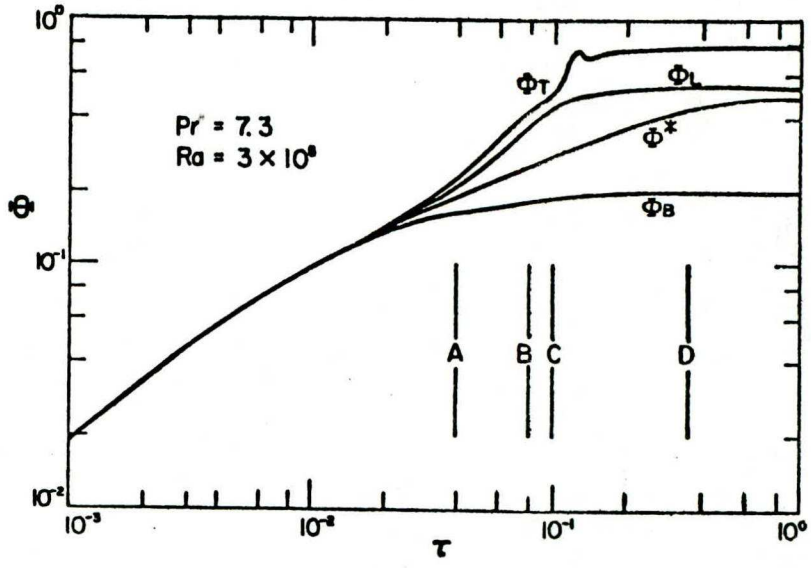

(d)

Fig. 5 Transient velocity profiles along X = 1 (a) and temperature profiles along Y = 0 (b) and X = 1 (c) and average wall heat flux distribution (d) for Pr = 7.3 , Ra = 3×10^5 and E = 2 at various times τ.

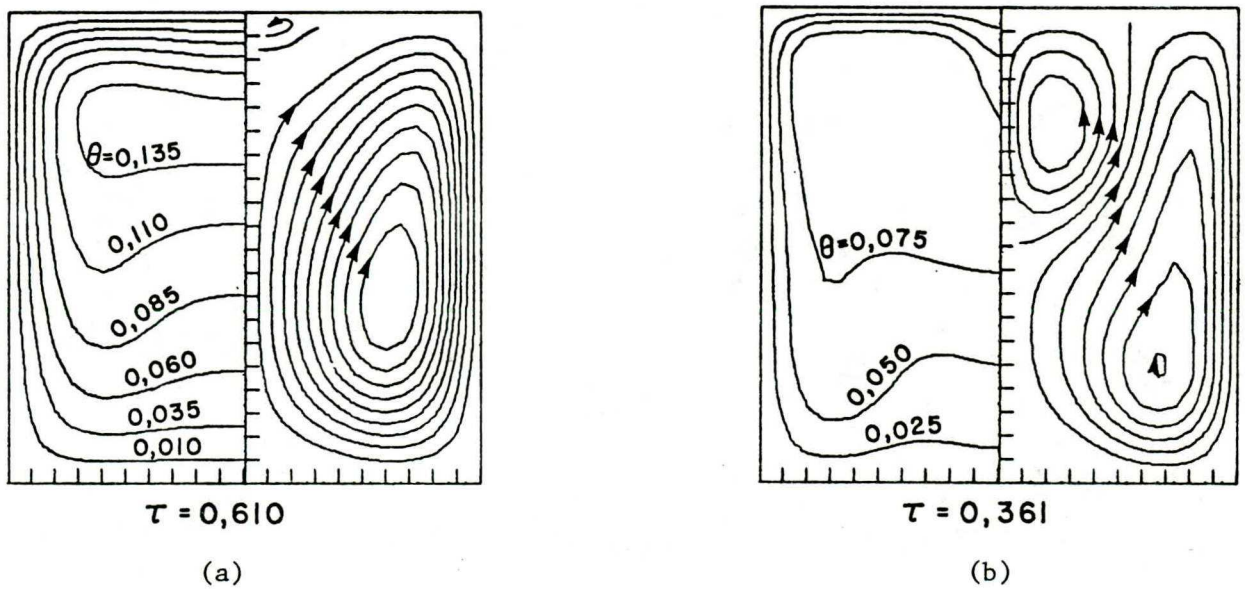

Fig. 6 Quasi-steady state streamline and isotherm fields for $Pr = .73$ and $E = 2$. The centerline and walls have value $\Psi = 0$. The values of Ra, Ψ_{max}, Ψ_{min} and $\Delta\Psi$ are

(a) $Ra = 5 \times 10^4$, $\Psi_{max} = 8.1$, $\Psi_{min} = -.02$, $\Delta\Psi = .81$;

(b) $Ra = 3 \times 10^5$, $\Psi_{max} = 15.0$, $\Psi_{min} = -9.5$, $\Delta\Psi = 2.45$.

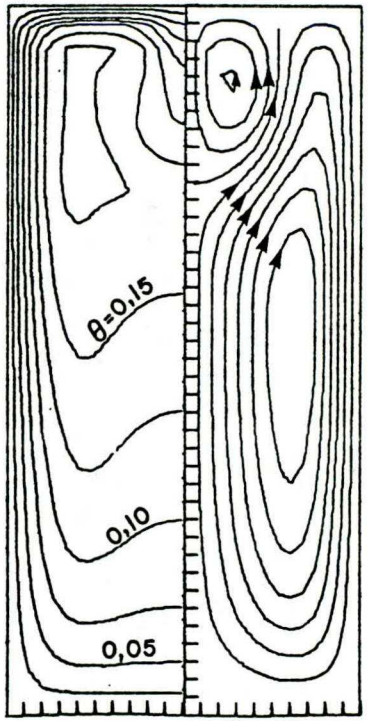

τ = 0,800

(a)

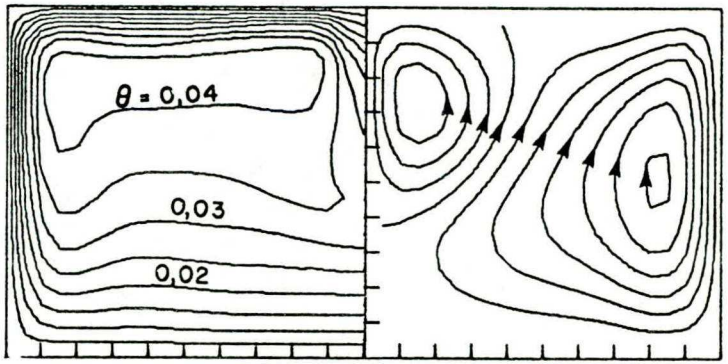

τ = 0,250

(b)

Fig. 7 Quasi-steady state streamline and isotherm fields for $Pr = 7.3$.
The centerline and walls have value $\Psi = 0$.
The values of Ra, E, Ψ_{max} , Ψ_{min} and $\Delta\Psi$ are
(a) $Ra = 7 \times 10^4$, $E = 4$, $\Psi_{max} = 16.0$, $\Psi_{min} = -7.1$, $\Delta\Psi = 2.3$;
(b) $Ra = 3 \times 10^6$, $E = 1$, $\Psi_{max} = 19.0$, $\Psi_{min} = -12$, $\Delta\Psi = 15.5$.

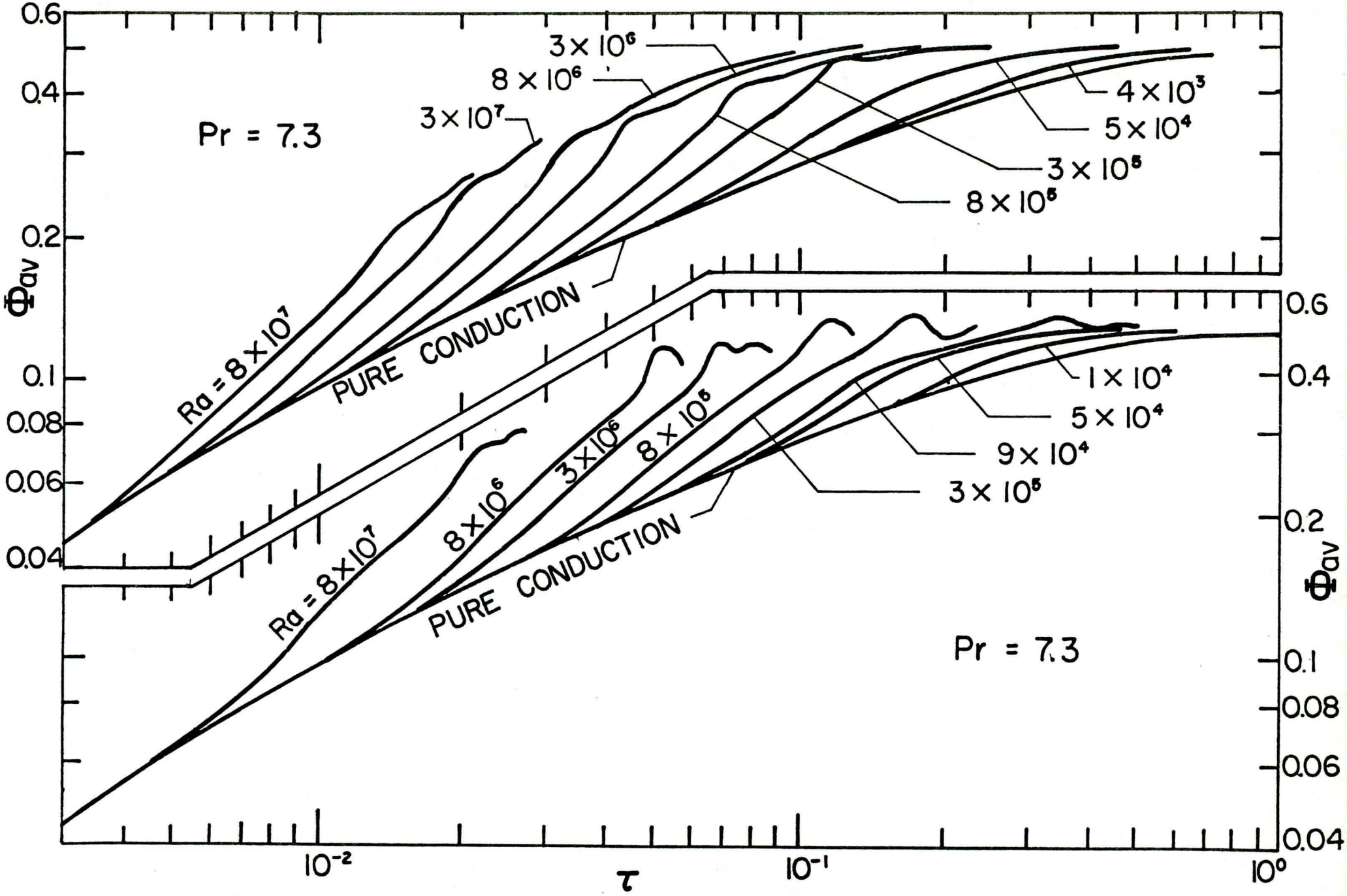

Fig. 8 Φ_{av} as a function of τ with Ra as a parameter for Pr = .73 and 7.3 .

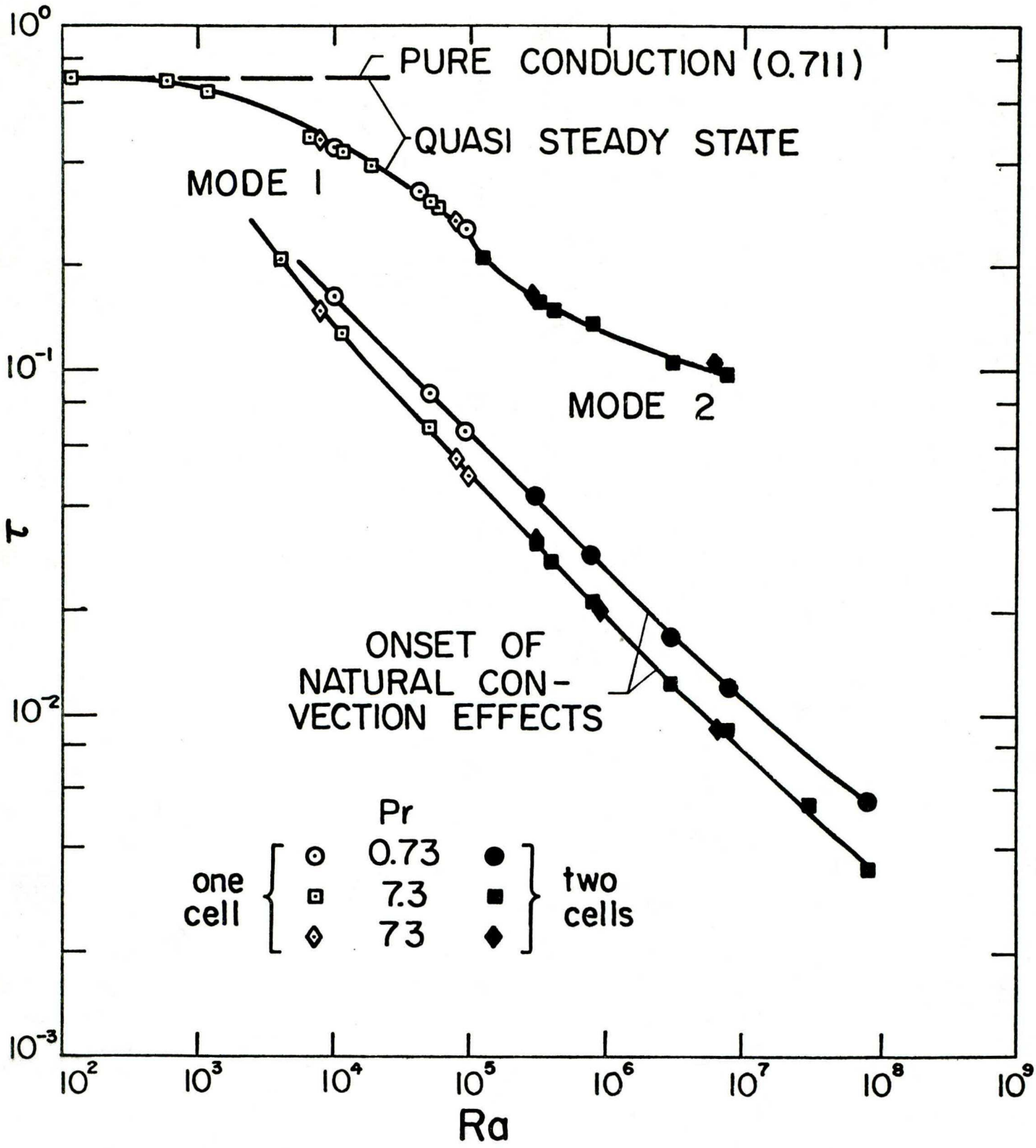

Fig. 9 Onset of natural convection effects and time to reach quasi-steady state.

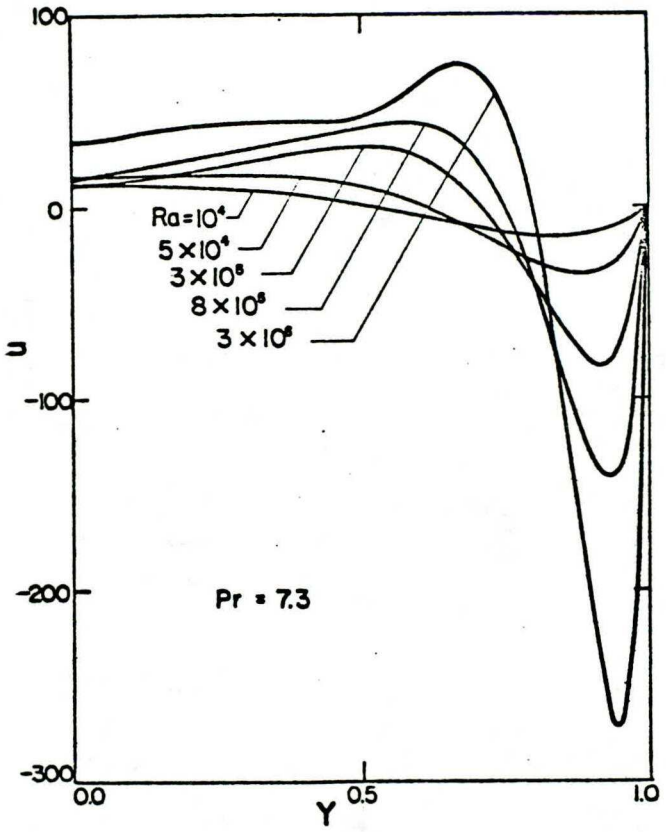

(a)

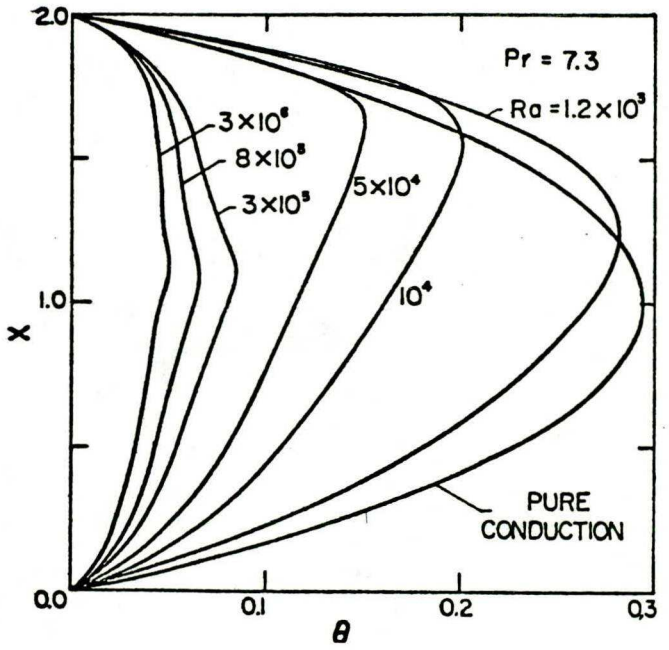

(b)

Fig. 10 Temperature profiles along Y = 0 (a) ; velocity profiles along X = 1 (b) , average wall heat flux (c) and typical temperature (d) distributions as function of Ra , at quasi-steady state for Pr = 7.3 and 73 .

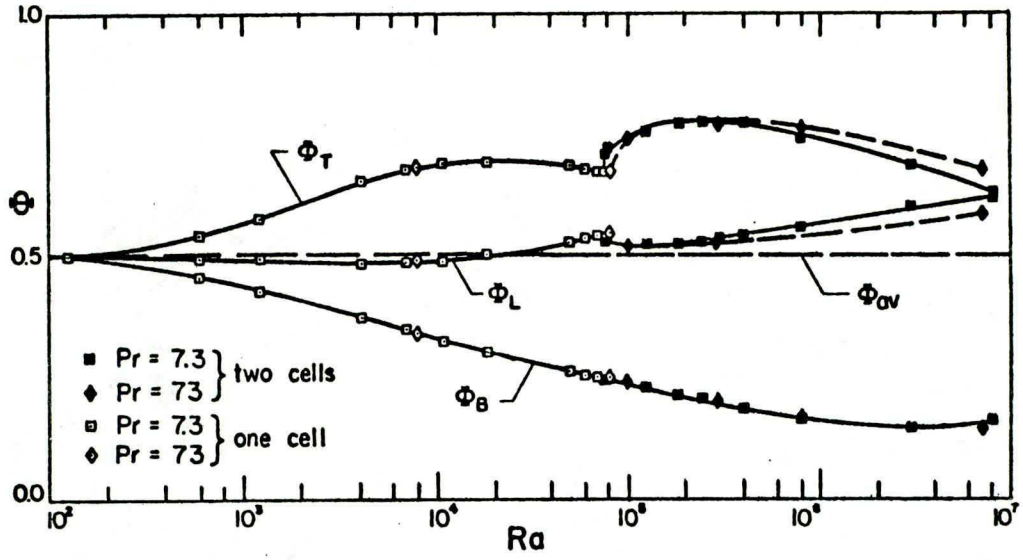

(c)

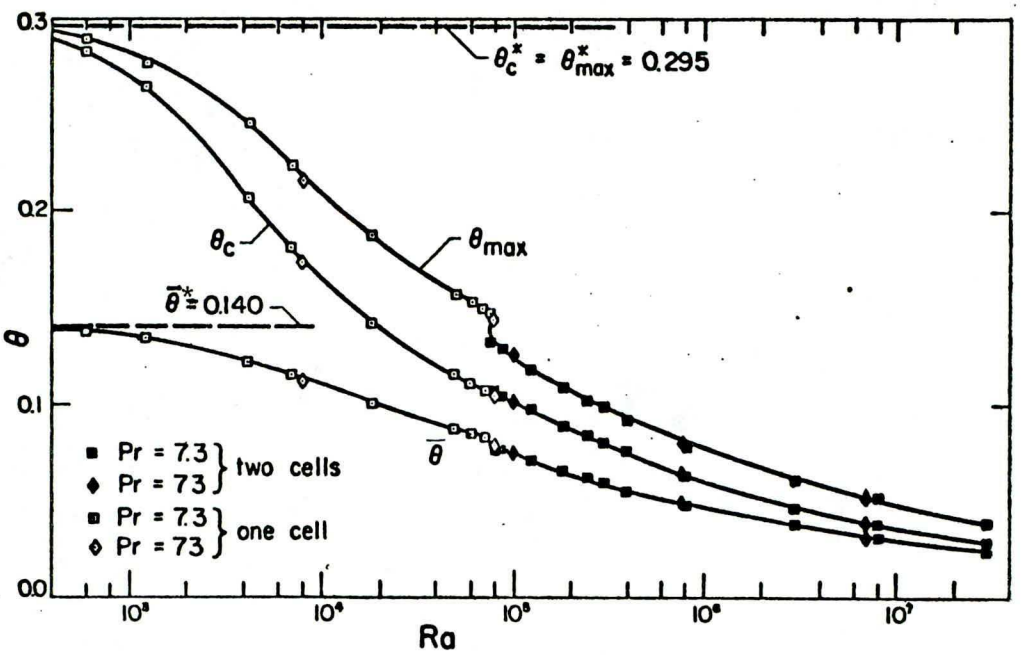

(d)

Fig. 10 Temperature profiles along Y = 0 (a) ; velocity profiles along X = 1 (b) , average wall heat flux (c) and typical temperature (d) distributions as function of Ra , at quasi-steady state for Pr = 7.3 and 73.

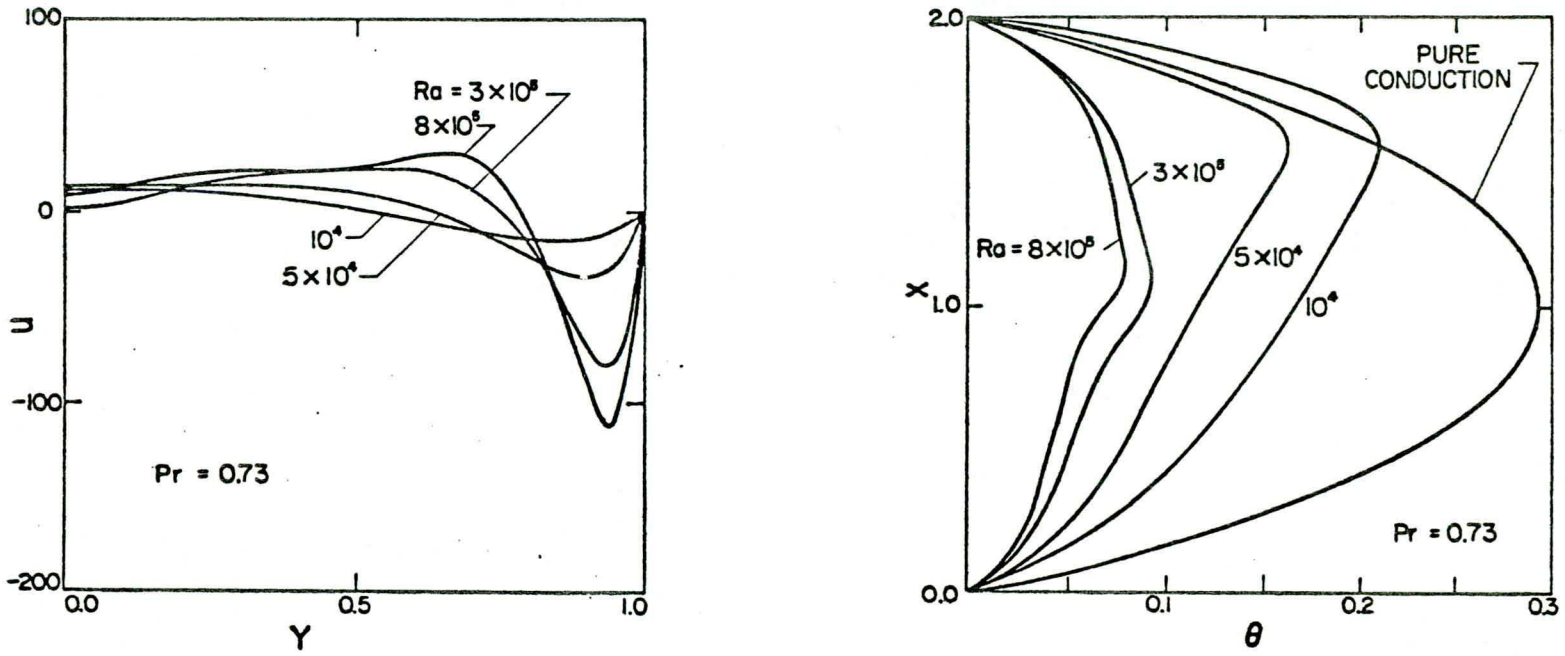

(a) (b)

Fig. 11 Temperature profiles along Y = 0 (a) , velocity profiles along X = 1 (b) , average wall heat flux (c) and typical temperature (d) distributions as function of Ra , at quasi-steady state for Pr = .73 .

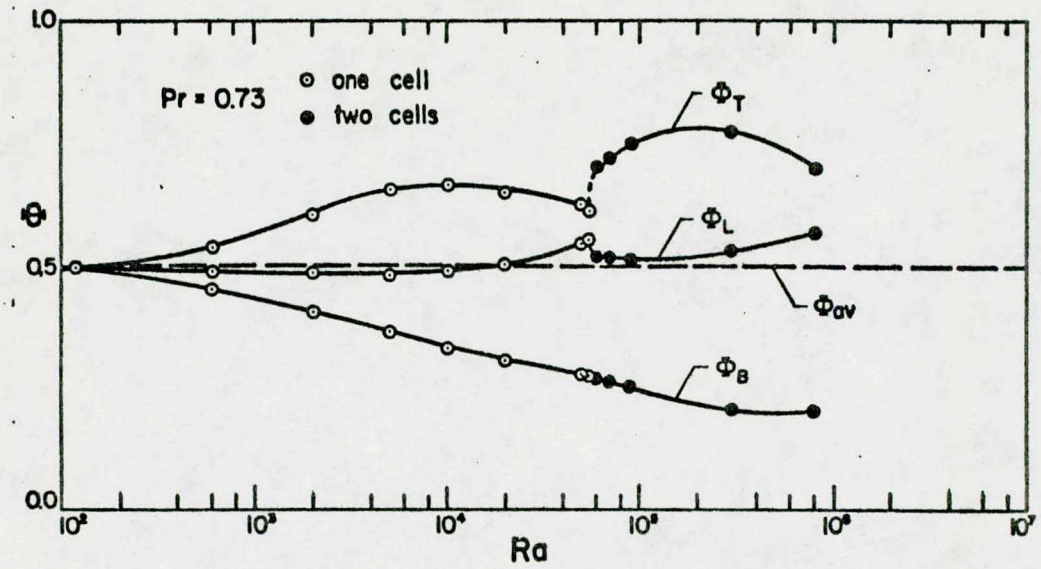

(c)

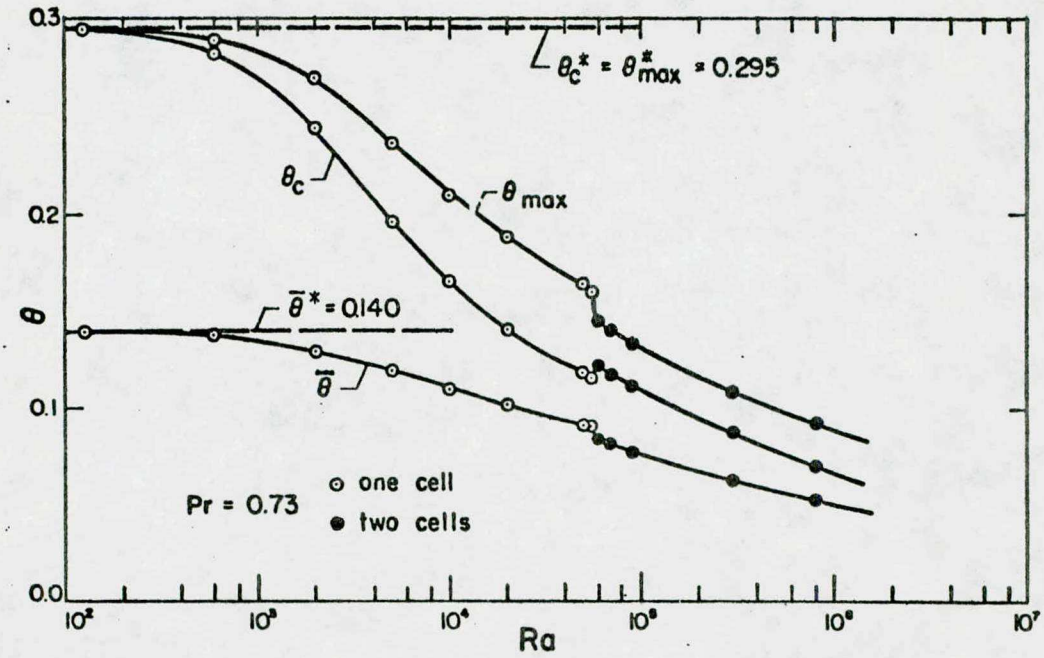

(d)

Fig. 11 Temperature profiles along Y = 0 (a), velocity profiles along Y = 1 (b) , average wall heat flux distributions (c) and typical temperature (d) distributions as function of Ra , at quasi-steady state for Pr = .73 .

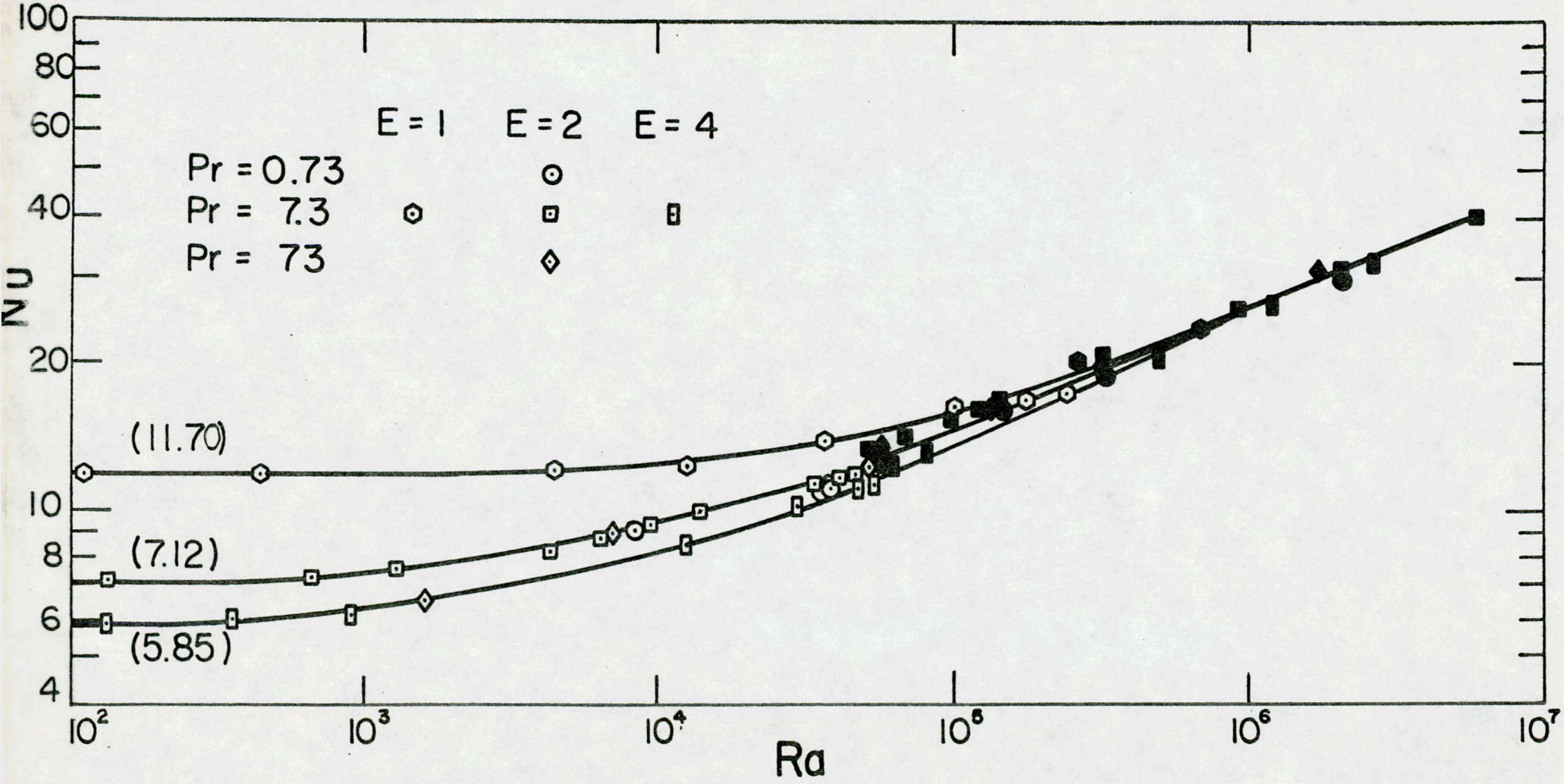

Fig. 12 Relationship between Nusselt number and modified Rayleigh number for the quasi-steady state.

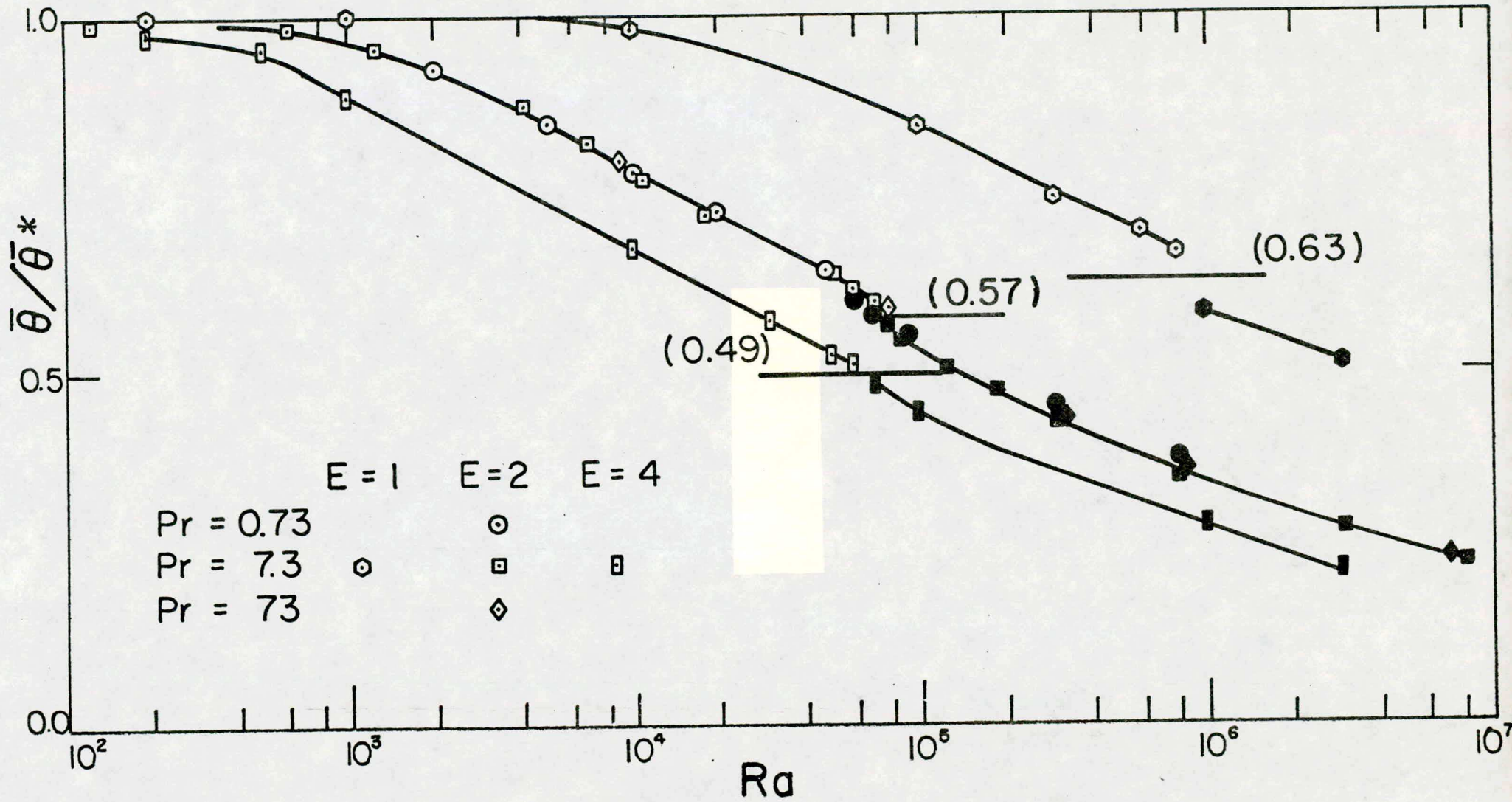

Fig. 13 Relationship between $\overline{\theta}/\overline{\theta}^*$ and Ra for E = 1 , 2 and 4.